Dynamic model for kinesin-mediated long-range transport and its local traffic jam caused by tau proteins

Woochul Nam and Bogdan I. Epureanu*
University of Michigan, Ann Arbor, Michigan 48105, USA
(Received 1 November 2016; published 17 January 2017)

In neurons, several intracellular cargoes are transported by motor proteins (kinesins) which walk on microtubules (MTs). However, kinesins can possibly unbind from the MTs before they reach their destinations. The unbound kinesins randomly diffuse in neurons until they bind to MTs. Then, they walk again along the MTs to continue their tasks. Kinesins repeat this cycle of motion until they transport their cargoes to the destinations. However, most previous models mainly focused on the motion of kinesins when they walk on MTs. Thus, a new model is required to encompass the various types of kinesin motion. We developed a comprehensive model and studied the long-range axonal transport of neurons using the model. To enhance reliability of the model, it was constructed based on multiphysics on kinesin motion (i.e., chemical kinetics, diffusion, fluid dynamics, nonlinear dynamics, and stochastic characteristics). Also, parameter values for kinesin motions are carefully obtained by comparing the model predictions and several experimental observations. The axonal transport can be degraded when a large number of binding sites on MTs are blocked by excessive tau proteins. By considering the interference between walking kinesins and tau molecules on MTs, effects of tau proteins on the axonal transport are studied. One of the meaningful predictions obtained from the model is that the velocity is not an effective metric to estimate the degradation of the transport because the decrease in velocity is not noticeable when the concentration of tau protein is not high. However, our model shows that the transport locally changes near tau molecules on MTs even when the change in the velocity is not significant. Thus, a statistical method is proposed to detect this local change effectively. The advantage of this method is that a value obtained from this method is highly sensitive to the concentration of tau protein. Another benefit of this method is that this highly sensitive value can be acquired with relatively low precision and low temporal resolution considering the time scale and length scale of the kinesin motion. This method can be used to estimate the condition of the axonal transport system.

DOI: 10.1103/PhysRevE.95.012405

I. INTRODUCTION

Motor proteins are responsible for the intracellular transport of a variety of cargoes such as mitochondria, neurotransmitters, and neurofilaments [1–4]. Among them, kinesins are highly processive motors [5] that walk from the cell body to synapses along biological tracks, i.e., microtubules (MTs). When a kinesin molecule unbinds from a MT, the unbound kinesin diffuses away from the MT. If there are few MTs, the unbound kinesin is unlikely to move close to MTs. Thus, the probability of unbound kinesins to rebind to one of MTs is very small. Under this circumstance, the transport cannot be continued after kinesins are released from MTs. However, neurons contain a large number of MTs in their long structures called axons, which connect their cell bodies and synapses. Thus, unbound kinesins in axons are highly likely to bind again to one of the MTs in a short time, and they walk again along the MT. Also, the axons are very long (10–100 μm) considering that kinesins unbind from MTs after they walk about 1μm [6,7]. Therefore, kinesins in axons repeatedly walk along MTs, unbind from MTs, diffuse (by Brownian motion) in cytoplasm, and bind to MTs to walk again. This cycle of kinesin motion is shown in Fig. 1. Also, the cycle of motion can be modified if other intracellular molecules are present on the binding sites of MTs.

To describe the long-range axonal transport in neurons, both the cycle of motion and effects of other molecules (present on MTs) should be considered. Because an elaborate model considering both the cycle and effects has not been developed yet, we propose an integrated model for the long-range transport in this paper. Our integrated model is created by introducing a method to calculate the diffusing motion (or the Brownian motion) of unbound kinesins, by developing a method capable of capturing the instant and the position of the binding to MTs, and by combining these methods with previously developed models for walking and unbinding.

Several proteins (e.g., tau protein, MAP1, MAP2, and MAP4) can bind to MTs [8–10]. Among these proteins, we focus on tau protein because several experiments showed that tau protein is closely related to neurodegenerative diseases [11–13]. When MTs are polymerized with tubulins, tau protein stabilizes the structure of MTs by binding to the inner surface of MTs [14–16]. However, if excessive tau molecules are provided when MTs are already stabilized, the excessive tau molecules can interrupt the motion of kinesins by binding to the outer surface of MTs on which kinesin molecules walk [17–21]. Hereafter, excessive tau protein (or molecule) is referred to as tau protein (or molecule). The distribution of tau molecules on the MTs should be characterized to consider effects of tau protein on kinesin-mediated transport. Previous experiments [17,22] suggested that the interaction between tau protein and MTs cannot be modeled with single chemical

*Corresponding author: epureanu@umich.edu

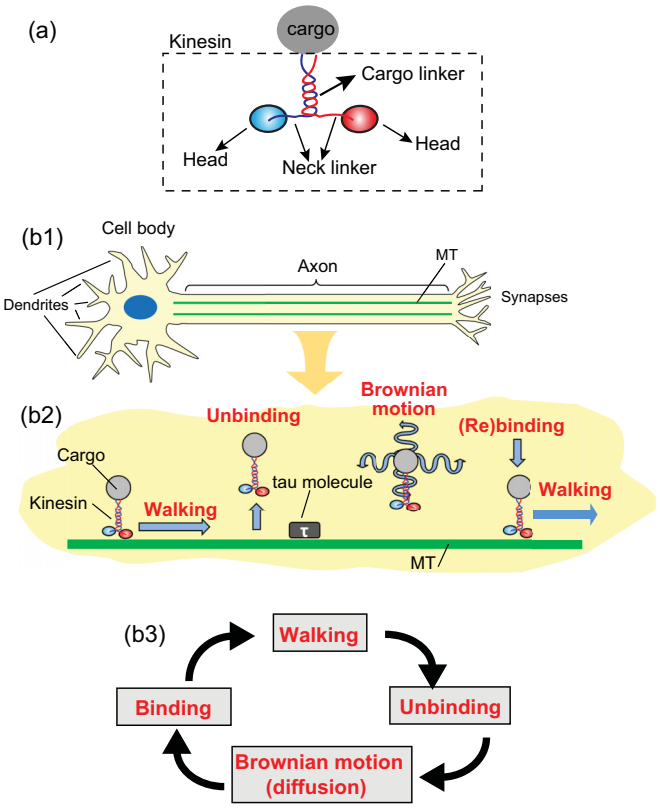

FIG. 1. Kinesin and axonal long-range transport. (a) The assembly of kinesin and cargo. (b1) The structure of a neuron composed of cell body, dendrites, axon, and synapses. (b2) Various types of kinesin motion in axonal transport. (b3) The cycle of kinesin motion.

kinetics. Several coupled chemical kinetics are necessary to consider the complicated interaction between tau protein and MTs. To this end, we considered three different interactions of tau protein and MTs. Then, parameter values corresponding to each interaction are obtained by comparing the results of our model to experimental data.

Several effects of tau protein on kinesin motion were observed in previous experiments. The walking motion of kinesins on the MTs slightly changes due to tau proteins [17,20]. However, both the binding of kinesins to MTs and their unbinding from MTs are affected considerably by tau proteins. The probability of kinesins to unbind from MTs increases considerably due to tau proteins [17–20]. Also, the probability of unbound kinesins to bind to the MTs decreases [21] if binding sites on MTs are occupied by tau molecules. Because our model is constructed to describe various motions of kinesins, these complicated effects of tau protein on the transport can be considered. Also, the parameters corresponding to the effects of tau protein were calculated based on the changes observed in the several experiments.

By using our generic model, we predicted an exciting (potential) phenomenon of axonal transport. When the concentration of tau protein is not high, the time required to transport a cargo along a 50-μm-long axon does not change considerably. However, the transport is delayed in front of tau clusters and accelerated behind tau clusters present on MTs. This local change takes place even when the transport is not delayed considerably. Therefore, this phenomenon can be useful to estimate the condition of MTs (i.e., the density of MTs in axons and the number of binding sites blocked by tau proteins). Because the size of kinesin molecules is very small, the position of cargoes (transported by kinesins) is captured in experiments instead of tracing the kinesin molecules. The position of cargoes randomly changes due to thermal fluctuations and the stochastic chemical reactions of kinesins. Thus, it is difficult to find local changes (resulted from tau clusters) from the randomly fluctuating motion of the cargo. Therefore, we propose a method to differentiate the local changes from the stochastic motion of the cargo. This method can be very useful because the value calculated by using the method varies noticeably upon the condition of MTs even when the degradation of the transport is insignificant.

II. MODEL

To describe kinesin-mediated long-range transport, various types of kinesin motion [depicted in Fig. 1(b)] are considered. Also, the binding of tau molecules to MTs and their effects on the kinesin motion are characterized to predict the corresponding changes in transport due to tau proteins.

A. Kinesin bound to a MT: Walking and unbinding

For kinesins bound to MTs, the walking motion, the unbinding, and the interaction between cargoes and kinesins are captured with previously developed mechanistic models [23–26]. The walking motion of a kinesin is determined by the period and direction of its step [5,27]. Its stochastic stepping period is calculated with a chemical kinetics on the binding of Adenosine triphosphate (ATP) to kinesin heads and the subsequent hydrolysis [23,24]. While a kinesin takes a step, one of its heads is bound to the MT and the other head moves by diffusion and a conformational change in its structure. The direction of a step is considered according to the previously developed model [26] which is capable of capturing the diffusing motion of the kinesin head. Kinesin heads are connected to neck linkers, as shown in Fig. 1(a). A nonlinear stiffness of the neck linker was also considered when capturing the diffusing motion of the head. The unbinding probability calculated in previous studies [25,26] is used to capture the stochastic instant of release from the MT. When a kinesin walks along a MT, the motion of its cargo is calculated with Stokes's law, i.e., $v_c = \frac{F_c}{6\pi r_c \eta}$, where v_c is the velocity of cargo, and F_c is the force acting on the cargo (transferred from the kinesin). This force can be calculated with the nonlinear stiffness of the cargo linker and the positions of the cargo and the kinesin. r_c is the radius of the cargo, and η is the viscosity of the fluid in the axon. Details on walking and unbinding are provided in our previous works [23–26].

B. Kinesin released from a MT: Brownian motion and rebinding

In neurons, cargoes transported by kinesins can be detached from MTs and move randomly until they rebind to MTs. When the cargo is unbound from the MT, both the position of the cargo and the position of the kinesin heads fluctuate

in a different fashion. Thus, different methods are applied to enhance the computation efficiency.

First, the diffusing motion of the cargo is calculated by updating the cargo position (center location and rotation) at every time step (in time marching) with stochastic variables corresponding to Brownian motion. Because the size of the cargo is much larger than the kinesin heads, it is assumed that the motion of the cargo is not affected by the thermal fluctuations of the kinesin molecule. Translational and rotational motions of the cargo have to be calculated because both of them change the distance between the kinesin head and MTs. That is because the kinesin (which is unbound from MTs) location changes when the cargo rotates. The location of the kinesin is important because it determines the rebinding rate. When a cargo with a radius of r_c moves due to thermal forces, the autocorrelations of the translational and rotational motions can be calculated as

$$\langle[\mathbf{x}_c(t+\Delta t)-\mathbf{x}_c(t)]^2\rangle = 2D_t\Delta t,$$
$$\langle[\boldsymbol{\theta}_c(t+\Delta t)-\boldsymbol{\theta}_c(t)]^2\rangle = 2D_r\Delta t, \quad (1)$$

where $D_t(=k_BT/6\pi r_c\eta)$ is the diffusion coefficient of the translational motion, $D_r(=k_BT/8\pi r_c^3\eta)$ is the diffusion coefficient of the rotational motion, and Δt is the time step. The translational motion of the unbound cargo is calculated using $x_c(t+\Delta t)=x_c(t)+\boldsymbol{r}_t(\Delta t)$, where $\boldsymbol{r}_t(\Delta t)$ is a vector with three elements. Each element is a stochastic variable that represents a random translation Brownian motion in the three-dimensional space. Each of the stochastic variables has a normal distribution with a zero mean value and a standard deviation (std) of $\sqrt{2D_t\Delta t}$. Likewise, the rotational motion of the unbound cargo is calculated using $\boldsymbol{\theta}_c(t+\Delta t)=\boldsymbol{\theta}_c(t)+\boldsymbol{r}_\theta(\Delta t)$, where $\boldsymbol{r}_\theta(\Delta t)$ is a vector with three elements. Each of the elements is a stochastic variable modeling one of the three rotations in the three-dimensional space. Each of the stochastic variables have normal distribution with a zero mean value and a std of $\sqrt{2D_\theta\Delta t}$. Different values of $\mathbf{r}_t$ and $\mathbf{r}_\theta$ are used at different time steps to capture the random motion. The Brownian motion of the cargo is confined by the cell membrane and the surface of the MTs, as shown in Fig. 2(a). The motion after the collision is calculated by assuming that the kinetic energy dissipation by collision is negligible.

Second, the method used for determining the diffusion of the cargo can be applied to the kinesin heads also. However, kinesin heads have a very high diffusion coefficient (i.e., $D_k=73.6\,\mu\text{m}^2/\text{s}$) [26] because of their small size (i.e., $7.5\times4.5\times4.5\,\text{nm}^3$). Considering that the std of the translational Brownian motion is $\sqrt{2D_t\Delta t}$, the motion of the unbound kinesin computed by time marching has to be calculated with a small time step of at most 1 ns (to calculate its position with a resolution of 1 nm). In addition, the time for the kinesin to complete its transport along long axons is on the order of 10–100 s. Hence, the very small time step results in many steps being required, and that results in very long computations. Thus, we developed a probability-based method to consider the binding of unbound kinesins to MTs. The proposed method is much faster because it does not require predicting the fast motion of the kinesin heads with the extremely short time steps.

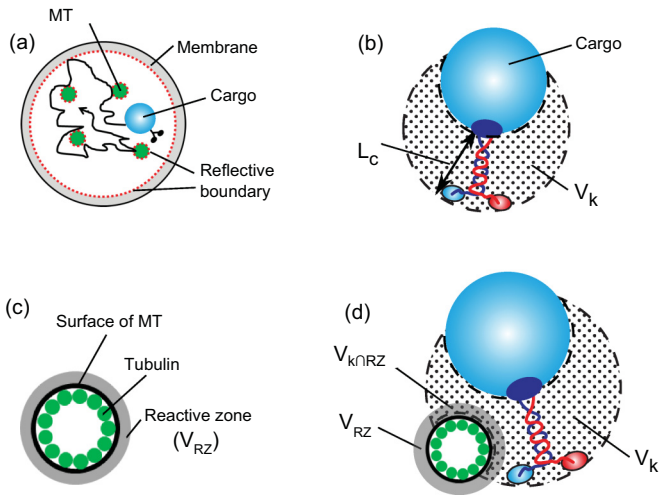

FIG. 2. Brownian motion and rebinding. (a) The Brownian motion depicted from the cross section of the axon. The dots in (b) indicate the spherical volume where the unbound kinesin heads can exist with spatially uniform probability distribution. (c) The cross section of the MT. The gray layer represents the reactive zone (volume V_{RZ}) of the MT. (d) A cargo with a kinesin (with free heads) in the proximity of a MT. $V_{K\cap RZ}$ is the intersection of the allowable space V_k of the unbound kinesin and the reactive zone.

The positions of unbound kinesin heads can be regarded to be constrained in the volume V_k because the kinesin is linked to the cargo by the cargo linker, as shown in Fig. 2(b). The spherical volume V_k has its center at the point where the kinesin attaches to the cargo. The radius of V_k is the length of the kinesin (L_c) in the absence of stretching force [28], namely, 60 nm. Note that the volume V_k is not spherical but it is a part of a spherical volume. V_k represents the volume of space where the unbound kinesin heads can exist with no mechanical interference between the kinesin head and the MTs. Thus, V_k does not contain volume inside the MTs (and does not pass though the MTs). In addition, V_k decreases when the cargo is closer to the MT, as shown in Fig. 2(d). Moreover, V_k decreases when the cargo is close to the membrane of the axon also. The unbound kinesin molecule fluctuates very fast, i.e., much faster than the cargo. Therefore, kinesin molecules can travel everywhere in the volume V_k during a given time period that is longer than the time scale of the diffusion of the kinesin. Hence, we can assume that the probability to find the kinesin heads at any position inside V_k during that time is the same, i.e., the probability of finding the kinesin heads is uniform over the volume V_k. This assumption is plausible because of the high diffusion coefficient of kinesin heads and tether behavior of the cargo linker (soft in bending, and stiff in stretching).

The binding of the (unbound) kinesin to MTs can be considered using a first order single-molecule kinetics. The equations governing the probability for single molecule kinetics have the same form as the equations governing the chemical reaction rate, as described in the study of Kou *et al.* [29]. For a chemical reaction composed of three states, they derived the chemical reaction rate equation by considering the concentrations of the molecule in each state as a state variable. Then, they

constructed the equation for the probabilities of the single molecule by converting the state variable (i.e., concentrations) in the rate equation into the probabilities. The same approach is used in our study to consider the binding of the (unbound) kinesin to MTs. The dynamics of rebinding can be described with two state variables (i.e., the rebinding probability P_{reb} and probability to remain in the unbound state P_{ubd}). The rate of change in the rebinding probability P_{reb} can be calculated with the transition rate k_{reb} from an unbound state to a bound state as

$$\frac{d}{dt}P_{\text{reb}} = k_{\text{reb}}P_{\text{unb}} = k_{\text{reb}}(1 - P_{\text{reb}}). \tag{2}$$

Note that k_{reb} also includes the effects of the MT numbers on the rebinding rate by allowing the value of k_{reb} to be changed by the position of the kinesin molecule relative to the MTs. It is assumed that the MT has a reactive zone covering the outer surface of the MT with thickness of 1 nm, as shown in Fig. 2(c). If the head of the unbound kinesin enters this region, the kinesin can bind to the MT. If the kinesin head is outside of the reactive zone, it is not able to bind to the MT. Thus, the k_{reb} is proportional to the probability that the kinesin head stays in the reactive zone. Then, the rate k_{reb} can be calculated as

$$k_{\text{reb}} = q_{\text{reb}}\frac{V_{\text{K}\cap\text{RZ}}(\mathbf{x}_c(t),\boldsymbol{\theta}_c(t))}{V_{\text{K}}}, \tag{3}$$

where $V_{\text{K}\cap\text{RZ}}$ is the intersection volume of V_K and V_{RZ}, as shown in Figs. 2(b)–2(d). $q_{\text{reb}}(= 1.3 \times 10^5\ \text{s}^{-1})$ is a parameter of the rebinding model. Experimental observations and a method to calculate the value of q_{reb} are provided in Sec. III. Note that $V_{\text{K}\cap\text{RZ}}$ changes over time because the unbound cargo moves by the thermal fluctuations. Thus, the value of k_{reb} has to be updated at every time step. The time step Δt is determined as 0.01 ms because the rebinding rate does not depend on Δt, if it is less than or equal to 0.01 ms.

C. Binding of tau molecules to MTs

The following behaviors of tau protein are considered its binding to MTs.

(1) When the molar ratio m_τ (= concentration of tau protein/concentration of tubulin dimer) is smaller than 0.2, almost all tau molecules bind to the MTs [17,22]. This molar ratio of 0.2 is also consistent with the stoichiometries obtained from other experiments [30–32]. Thus, a single tau molecule is assumed to occupy four tubulin dimers in a square layout [i.e., two by two, as shown in Fig. 3(a)] because one tau molecule interacts with two protofilaments [33,34]. This interaction is also consistent with previous observations [35] which suggest that tau molecules bind both along and across protofilaments.

(2) Some tau molecules fail to bind on the MTs when m_τ is higher than 0.2 [22]. This suggests that tau proteins are unlikely to bind to tubulins which are already occupied by single tau molecules.

(3) Tau clusters are observed on the MT for high values of m_τ [17,22,36]. Note that if two or more tau molecules bind to the same location on the MT, those tau proteins are referred to as a tau cluster in this study. Once a tau molecule succeeds to bind to tubulins where another tau molecule is already bound (even if the probability to bind to those tubulins is small),

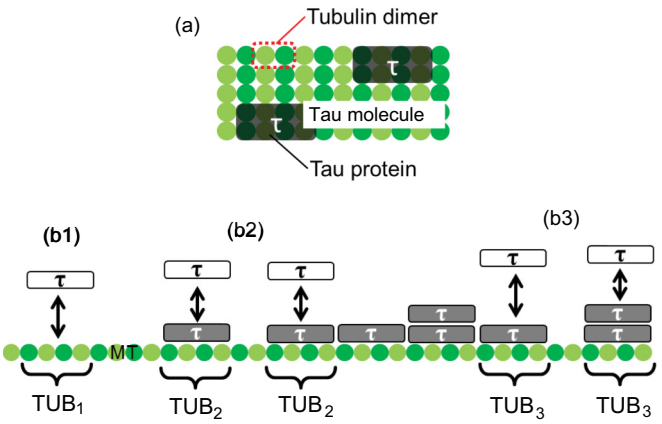

FIG. 3. Binding of tau molecules to tubulins. (a) The assumed configuration of bound tau molecules. (b) Three distinct types of interaction between free tau molecules and tubulins or bound tau molecules.

the two tau molecules act as a seed to which other free tau molecules can easily bind. This is consistent with observations that tau dimers function as building blocks in the formation of aggregates of tau molecules in the absence of tubulins [37].

(4) For large values of m_τ, the ratio of unbound tau molecules to bound tau molecules increases with m_τ. To capture this behavior, it is assumed that tau molecules can bind to tubulins only when the number of tau molecules bound on the tubulins is equal to or less than N_{max}.

To consider the interaction between tubulins and tau molecules, tubulins on MTs are classified into three types. The first type (TUB_1) is tubulins with no tau molecules attached, as shown in Fig. 3(b1). The second type (TUB_2) is tubulins which already have one bound tau molecule and the adjacent sites have one or no tau molecule, as shown in Fig. 3(b2). The third type is the tubulins (TUB_3) where tau clusters are located, as shown in Fig. 3(b3). TUB_3 also includes the tubulins adjacent to tau clusters. Thus, TUB_3 represents the binding sites of the MT affected by tau clusters. Then, the probability of tau molecules to bind to a MT can be determined with a coupled single molecule kinetics shown in Fig. 4.

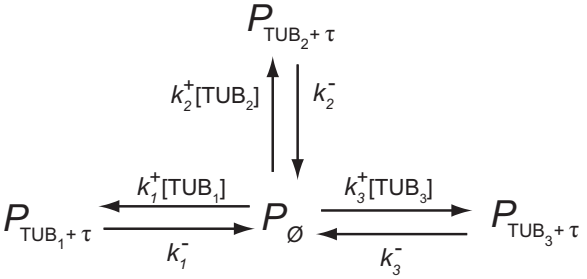

FIG. 4. Single molecule kinetics of tau molecules and tubulins. P_ϕ is the probability that the tau molecule is unbound, $P_{\text{TUB}_{1-3}+\tau}$ are the probabilities that the tau molecule binds to tubulins TUB_{1-3}, k_{1-3}^+ are the binding rate constants, k_{1-3}^- are the unbinding rate constants, and $[\text{TUB}_{1-3}]$ are the concentrations of TUB_{1-3}.

Then, the probabilities can be calculated using the following equations:

$$\begin{aligned}
\frac{d}{dt}P_{\mathrm{TUB}_1+\tau} &= k_1^+[\mathrm{TUB}_1]P_\phi - k_1^- P_{\mathrm{TUB}_1+\tau},\\
\frac{d}{dt}P_{\mathrm{TUB}_2+\tau} &= k_2^+[\mathrm{TUB}_2]P_\phi - k_2^- P_{\mathrm{TUB}_2+\tau},\\
\frac{d}{dt}P_{\mathrm{TUB}_3+\tau} &= k_3^+[\mathrm{TUB}_3]P_\phi - k_3^- P_{\mathrm{TUB}_3+\tau},\\
\frac{d}{dt}P_\phi &= -\frac{d}{dt}P_{\mathrm{TUB}_1+\tau} - \frac{d}{dt}P_{\mathrm{TUB}_2+\tau} - \frac{d}{dt}P_{\mathrm{TUB}_3+\tau}.
\end{aligned} \tag{4}$$

By defining the ratio of the binding rate constant and unbinding rate constant as affinity $K_{a,1-3} = \frac{k_{1-3}^+}{k_{1-3}^-}$, the probabilities at equilibrium can be obtained by solving the following equations:

$$\begin{aligned}
P_{\mathrm{TUB}_1+\tau} &= K_{a,1}[\mathrm{TUB}_1]P_\phi,\\
P_{\mathrm{TUB}_2+\tau} &= K_{a,2}[\mathrm{TUB}_2]P_\phi,\\
P_{\mathrm{TUB}_3+\tau} &= K_{a,3}[\mathrm{TUB}_3]P_\phi,\\
P_\phi + P_{\mathrm{TUB}_1+\tau} + P_{\mathrm{TUB}_2+\tau} + P_{\mathrm{TUB}_3+\tau} &= 1.
\end{aligned} \tag{5}$$

The following procedure is used to determine if a tau molecule binds to MTs and to determine the location of the binding:

(1) $[\mathrm{TUB}_1]$ is determined as the concentration of tubulin dimers of the MTs. $[\mathrm{TUB}_2]$ and $[\mathrm{TUB}_3]$ are zero.

(2) P_ϕ and $P_{\mathrm{TUB}_{1-3}+\tau}$ are calculated using Eq. (5).

(3) A random number $r_{\tau,b}$ between zero and one is generated.

(4) If $r_{\tau,b}$ is less than P_ϕ, the tau molecule fails to bind to the MT. If $P_\phi \leqslant r_{\tau,b} < P_\phi + P_{\mathrm{TUB}_1+\tau}$, then the tau molecule binds to TUB_1. If $P_\phi + P_{\mathrm{TUB}_1+\tau} \leqslant r_{\tau,b} < P_\phi + P_{\mathrm{TUB}_1+\tau} + P_{\mathrm{TUB}_2+\tau}$, then the tau molecule binds to TUB_2. Otherwise, the tau binds to TUB_3.

(5) When it is determined that the tau molecule is bound to the MT, another random number is generated to determine the binding location among the tubulins of the selected type.

(6) The new values of $[\mathrm{TUB}_{1-3}]$ are calculated based on the binding of the tau molecule.

The calculations from step 2 to step 6 are repeated again for every tau molecule with different random numbers.

The values of affinities are obtained as $K_{a,1} = 3\ \mu\mathrm{M}^{-1}$, $K_{a,2} = 3 \times 10^{-3}\ \mu\mathrm{M}^{-1}$, and $N_{\max} = 12$ by using the experimental data [17,22]. If $K_{a,3} \geqslant 10\ \mu\mathrm{M}^{-1}$, the effects of $K_{a,3}$ on the binding ratio of tau molecules on MTs, on the number of tau clusters, and on the distance between tau clusters are negligible. Thus, a value of $10\ \mu\mathrm{M}^{-1}$ is used for $K_{a,3}$. A detailed description on the method used to determine the values of these parameters is provided in Sec. III. Figure 5(a) shows the binding ratio of tau molecules to MTs. The growth of tau clusters and stochastic characteristics of our model regarding the binding of tau proteins on MTs are shown in Fig. 5(b) with four different examples (or realizations) of tau protein accumulation on a MT.

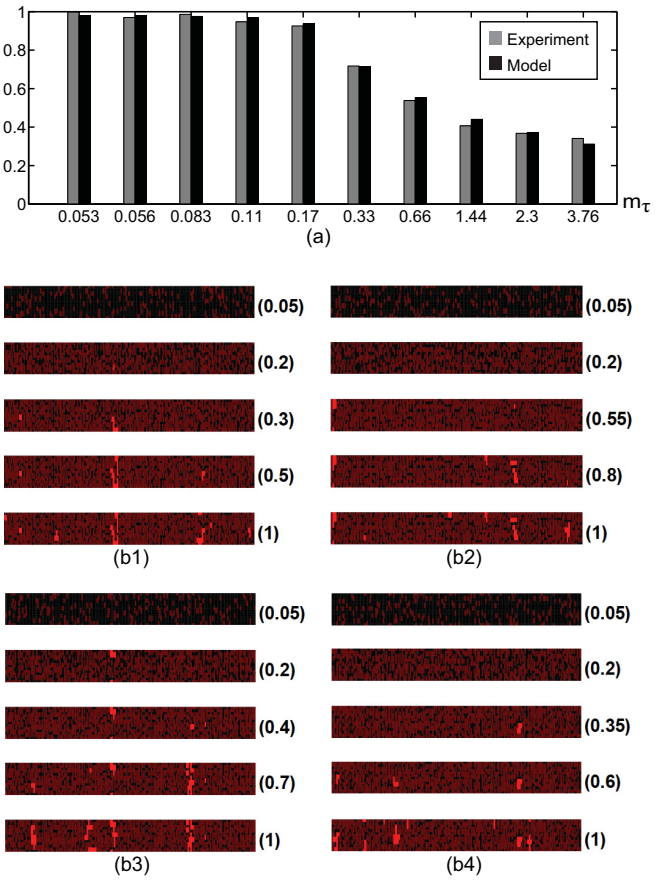

FIG. 5. Model prediction on the binding of tau molecules to MTs. (a) The binding ratio of tau molecules to MTs is shown over m_τ. (b) Tau molecules bound on a MT. Each image is a rectangle that represents the surface of the MT. Each group of images shows the evolution of tau molecules on the surface of a MT over m_τ from $m_\tau = 0.05$ to 1. Tubulins with no tau molecules are depicted with black dots, and tubulins with single tau are described with dark dots (or dark red). Lighter dots (or light red) are tubulins with two or more tau molecules (tau clusters). The locations of tau clusters are different in each of the groups of images (b1)–(b4) because of the stochastic characteristics on the binding of tau molecules.

D. Interference between kinesins and tau molecules

Tau molecules affect several dynamics of kinesin. First, the walking of kinesins is changed by tau molecules bound to MTs. The velocity of single kinesins increases by about 10% in the presence of tau proteins [17]. Moreover, the adenosine triphosphatase (ATPase) of kinesins is accelerated when kinesins meet tubulins where single tau proteins are attached [20]. This suggests that tubulins occupied by single tau proteins do not act as obstacles to kinesins. The accelerated ATPase by tau proteins is incorporated in our model by increasing the turnover rate in the ATPase by 10% when kinesin heads are bound on tubulins where single tau molecules are attached.

The probability that a kinesin unbinds from a MT increases when it encounters tau clusters [17,19,20]. The increase in the unbinding probability is determined by two probabilities: the probability (P_{int}) that the kinesin head collides with the tau clusters and the probability ($P_{\mathrm{ub,cnt}}$) of the kinesin to unbind when its head collides with the tau clusters. P_{int} can be obtained

by using the model developed in our previous study [26]. The value of $P_{\mathrm{ub,cnt}}$ is obtained as 3.2 nm/ms using experimentally observed run length (RL), the distance of kinesin molecules to walk before they are released from the MTs, in the presence of tau molecules [17]. A detailed description on the method used to determine the value of $P_{\mathrm{ub,cnt}}$ is provided in Sec. III.

The effect of tau molecules on the binding of free (unbound) kinesins to a MT is also considered. The binding rate of kinesins is observed to decrease over the concentration of tau protein [17,21]. Thus, it is assumed that unbound kinesins cannot bind to tubulins occupied by tau clusters. Note that this is consistent with the previously mentioned hypothesis that tau clusters act as obstacles for the heads of walking kinesins. Even if a tubulin is not occupied by tau clusters, the unbound kinesins are still unlikely to bind to that tubulin if the neighboring tubulins on the left and on the right (with respect to the direction of kinesin motion) are occupied by tau clusters; the space is not enough for the heads to reach that site. Thus, it is assumed that unbound kinesins cannot bind to such tubulins. The same assumption is made for where the neighboring tubulins in the front and the back are occupied by tau clusters. The binding rate of tau molecules to MTs obtained with these assumptions is similar to experimental data [17].

III. PARAMETER VALUES

To establish a reliable model, the values of the parameters are obtained based on the various experimental observations. Parameters regarding walking and unbinding are provided in our previous studies [25,26]. Details on the other parameters regarding the binding (q_{reb}), interaction between tau protein and MTs ($K_{a,1-3}$ and $N_{\max}$), and the interference between walking kinesin molecule and tau molecule on MTs ($P_{\mathrm{ub,cnt}}$) are explained in this section.

The value of the parameter (q_{reb}) regarding binding is obtained using the binding rate of kinesin molecules in the absence of tau proteins. Gilbert *et al.* [38] mixed free kinesins and MTs to measure the concentration of kinesins bound to MTs over time. Then, they calculated the binding rate of kinesins for various concentrations of tubulins. To calculate binding rate from the model, one MT is located at the center of the cylinder. The volume of the cylinder is determined so that the concentration of tubulin in the cylinder is the same as the concentration used in experiments. The Brownian motion of the kinesin is considered using D_t, D_r, and $\mathbf{r}_{\mathrm{ndr}}$. Cargoes with the radius 9.6 nm are used because this value corresponds to a hydrodynamic radius of kinesins measured in previous experiments [39]. The probability of binding to the MT is predicted using Eqs. (2) and (3). Then, several kinesins are randomly distributed inside the cylinders. Next, times for those kinesins to bind to the MT are predicted. The mean binding rate of kinesins is calculated by averaging the times. The binding rate calculated from the model is similar to the values measured in the experiment for various concentrations of tubulins for $q_{\mathrm{reb}} = 1.3 \times 10^5\ \mathrm{s}^{-1}$, as shown in Fig. 6(a).

The parameters ($K_{a,1-3}$, $N_{\max}$, and $P_{\mathrm{ub,cnt}}$) are identified using experiments [17,22] regarding the binding of tau molecules to MTs and several effects of tau proteins on the binding rate of unbound kinesins, and the RL of kinesins. Dixit *et al.* [17] used a very small concentration (50 nM) of dimer tubulins compared to their concentration in cells ($\simeq$20 μM). The binding rate of tau molecules to MTs is low for such small concentration of tubulins. To compensate this slowed reaction rate, they lowered the ionic strength in the assay. They reported that almost every tau molecule in the assay binds to the MTs when m_τ is small. Thus, it is difficult to determine the value of $K_{a,1}$ precisely using their results. Hence, in the model, a large number (1000 nM^{-1}) is used for $K_{a,1}$. Then, the number of bound tau molecules and the binding rate of kinesins are calculated with this model for various $K_{a,2}$, $K_{a,3}$, and $N_{\max}$. When $K_{a,2} = 7 \times 10^{-3}\ \mathrm{nM}^{-1}$, $K_{a,3} \geqslant 2\ \mathrm{nM}^{-1}$, and $N_{\max} = 12$, the binding of tau and binding rate of unbound kinesins have similar values to the experimental results obtained by Dixit *et al.*

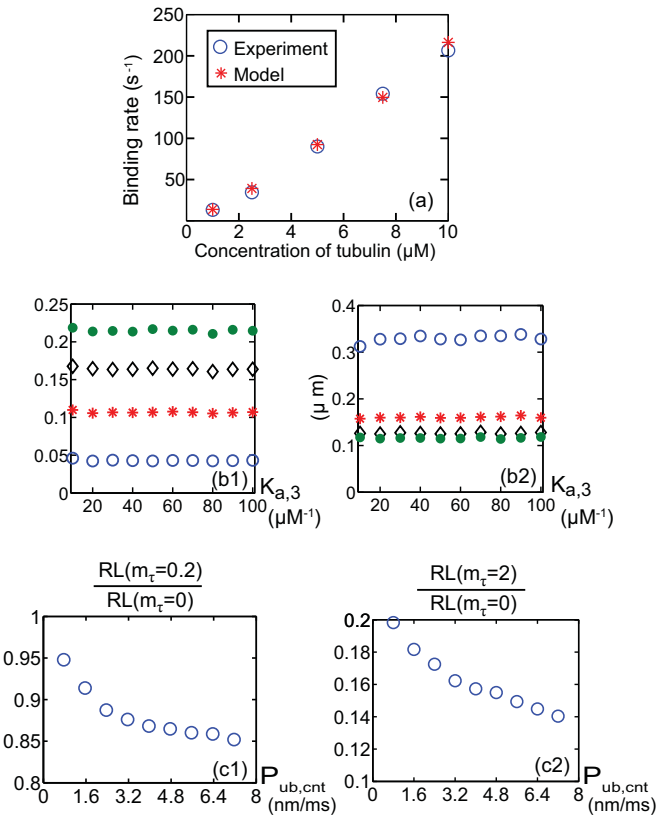

FIG. 6. Obtaining of the values of the parameters. (a) The binding rate of kinesins to MTs for various concentrations of tubulins. (b) The effects of $K_{a,3}$ on the distribution of molecules on the MTs are shown. (b1) Ratios of the number of tubulins occupied by two or more tau molecules to the number of tubulins of MTs over various $K_{a,3}$. The hollow circles, stars, diamonds, and filled circles denote the ratios for $m_\tau = 0.5$, 1, 1.5, and 2, respectively. (b2) Average distance between tau clusters. (c) The ratios of the RL in the presence of tau proteins and the RL in the absence of tau proteins. The ratio is obtained from the model for various $P_{\mathrm{ub,cnt}}$. (c) The changes in the RL due to the parameter $P_{\mathrm{ub,cnt}}$. (c1) RL ratios for $m_\tau = 0.2$; this ratio was observed to be 0.87 in previous experiments. (c2) RL ratios for $m_\tau = 2$, and this ratio was observed to be 0.16 in previous experiments. Therefore, the value of $P_{\mathrm{ub,cnt}}$ is determined as 3.2 nm/ms where model predictions match experimental observations.

The RL of kinesins in the presence of tau proteins [17] is used to obtain the value of the parameter regarding the unbinding probability $P_{\mathrm{ub,cnt}}$. This is the probability of the kinesin to unbind from the MT when the kinesin contacts a tau cluster. When m_τ is 0.2 or 2, the RL of kinesins decreases to 87or 17% of the RL in the absence of tau protein. When $P_{\mathrm{ub,cnt}} = 3.2\,\mathrm{nm/ms}$, the model predicts similar RLs, as shown in Fig. 6(c).

It is assumed that the changes in $N_{\max}$ and $P_{\mathrm{ub,cnt}}$ due to the concentration of tubulin are very small. Thus, the values for $N_{\max}$ and $P_{\mathrm{ub,cnt}}$ obtained using Dixit *et al.* [17] are used in our model. However, $K_{a,1-3}$ can be affected considerably by the concentration of tubulins and ionic strength. Therefore, the values of $K_{a,1-3}$ obtained from [17] can be different from their values in cells. Thus, the values of $K_{a,1-3}$ are obtained again by using the experimental data of Ackmann *et al.* [22] because the concentration of tubulins and ionic strength of their experiments are similar to those in cells. $K_{a,1} = 3\ \mu\mathrm{M}^{-1}$, $K_{a,2} = 3 \times 10^{-3}\ \mu\mathrm{M}^{-1}$, and $K_{a,3} \geqslant 10\ \mu\mathrm{M}^{-1}$ give similar results to the experimental results, as shown in Fig. 5(a). If $K_{a,3} \geqslant 10\ \mu\mathrm{M}^{-1}$, the effects of $K_{a,3}$ on the number of tau clusters and on the distance between tau clusters are negligible as shown in Fig. 6(b). Thus, a value of $10\ \mu\mathrm{M}^{-1}$ is used for $K_{a,3}$ in this study.

IV. RESULTS

In this study, the motion of a small cargo (with a diameter of 50 nm) transported by single kinesins is investigated. A previous experimental study revealed that the equivalent viscosity of the cytoplasm in neurons varies upon the diameter of cargoes [40]. According to those results, the equivalent viscosity for the cargo (with a diameter of 50 nm) is tenfold that of the viscosity of water. The axon is modeled as a single cylinder with a constant radius, 1 μm (average diameter of axons in the brain) [41], along its length. The MTs in the axon are aligned with the axis of the axon. Every MT has the same length as that of the axon, and they are distributed, as shown in Fig. 7(a).

A. Transport velocity

Because the Brownian motion and rebinding can occur several times during a long-range transport, a transport velocity is different from the walking velocity of the kinesin. A large number $N_t(= 200)$ of transport processes are computed and used to obtain the value of the transport velocity. Each of these transport processes is a different cargo moving along a different axon. Thus, a new distribution of tau proteins on the MT is created for each of these 200 transport processes. The distribution is created because the binding of tau protein on the MT is stochastic. The time required for the cargo to reach the end of the axon is calculated for each transport process. The transport velocity is obtained by dividing the transport distance (50 μm) by the mean value of the transport time. To predict the effects of MT density and concentration of tau protein $[\tau]$ on the transport of cargoes, the velocity of long transport (50 μm) is calculated. The number of MTs (N_{MT}) in axons is varied from one to six. A value of $N_{\mathrm{MT}} = 1$ in an axon of 1-μm diameter corresponds to the approximate density of MTs in pathological neurons from Alzheimer's disease patients ($1.2/\mu\mathrm{m}^2$) [42]. The MT density for $N_{\mathrm{MT}} = 6$ is similar to the MT density in healthy neurons ($7.1/\mu\mathrm{m}^2$).

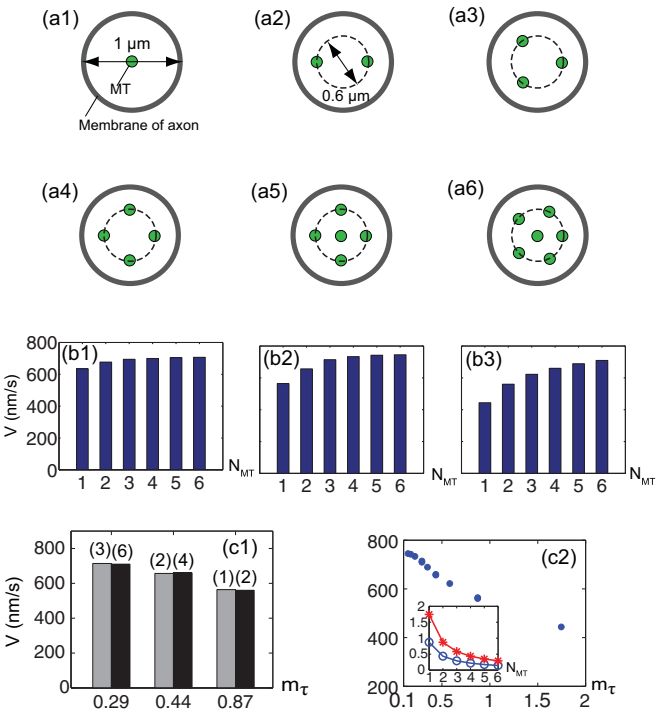

FIG. 7. Average velocity of cargoes. (a1)–(a6) The arrangement of MTs at the cross section of the axon. (b1), (b2), and (b3) The average velocities corresponding to $[\tau] = 0$, 3, and 6 μM, respectively. (c1) Velocities in axons with the same m_τ. However, $[\tau]$ and N_{MT} of the axons are different. The velocity for $[\tau] = 3\ \mu$M is presented by the gray bars. The black bars denote the velocity corresponding to $[\tau] = 6\ \mu$M. The numbers in parentheses indicate N_{MT}. (c2) The velocities over m_τ. Circles in the inset graph represent m_τ corresponding to $[\tau] = 3\ \mu$M, and asterisks denote m_τ corresponding to $[\tau] = 6\ \mu$M.

The velocity predicted by this model has the following features. First, the transport velocity along a healthy axon (i.e., no tau molecules and high density of MTs, $N_{\mathrm{MT}} = 6$) is very similar to a normal walking velocity of 800 nm/s of kinesins [43], as shown in Fig. 7(b1). However, the long-range transport can be delayed because the walking of kinesins does not take place when they are not bound to MTs. However, the delay is negligible in healthy axons because the unbound kinesins can bind to one of the MTs in a very short time. Second, the change in the transport velocity over MT density is considerable only when the axon contains a large concentration of tau protein, as shown in Fig. 7(b). Also, the effects of $[\tau]$ on the velocity are not noticeable if the number of MTs is sufficient. Lastly, the velocity in the presence of tau molecules can be determined by a single variable, namely, m_τ proportional to the ratio of $[\tau]$ and N_{MT} even though the motion of the kinesins is changed by both variables ($[\tau]$ and N_{MT}). Figure 7(c1) shows that velocities for different $[\tau]$ and N_{MT} are similar if m_τ has the same value. This feature can also be observed from the strong correlation between velocity and m_τ, as shown in Fig. 7(c2).

B. Motion of the cargo near tau clusters

The changes in transport velocity due to tau protein are not noticeable unless the axon has a small number of MTs and a large concentration of tau protein. However, the motion of kinesins near tau clusters is significantly disturbed. Thus, we investigated the use of this disturbance to estimate the condition of MTs. If kinesins encounter tau clusters, they bypass the cluster, or they are released from the MT. When a kinesin is unbound due to interference with tau clusters but diffuses forward, the motion of its cargo is not disturbed by the cluster. However, if the kinesin diffuses backward and rebinds to the MT, then the kinesin walks along the MT and encounters the tau cluster again, as depicted in Fig. 8(a). As a consequence, the motion of the cargoes is delayed when they encounter tau clusters.

However, various stochastic behaviors of kinesins also cause local delays in transport even when the kinesin is not close to tau clusters. Therefore, a new metric is required to distinguish the delay originating from tau clusters and other delays induced by the stochastic motion of kinesins. If a large number of transport processes are averaged, stochastic characteristics of kinesin behavior can be canceled out. Thus, a large number $N_t(=200)$ of transport processes are simulated for a single axon. Because 200 transport processes are accomplished in the same axon, the distribution of tau protein on the MTs is also the same in these 200 transport processes. Then, the probability of a cargo to be present at any location along the axon at any given time (i.e., the spatial probability distribution) is estimated. Specifically, the position of the cargo is captured with a constant sampling time (0.1 s) in this paper. The position of the cargo in the captured images is classified with a 1-μm resolution. When a cargo is present at the same location for a longer period, then the probability of the cargo to be present at that location is higher. If there are no spatial changes in the properties affecting the motion of cargoes along the axon (i.e., viscosity, temperature, diffusivity, or ATP concentration), the cargoes spend equal time in each section of the axon. Then, the probability distribution is spatially uniform. Otherwise, the probability distribution fluctuates along axons.

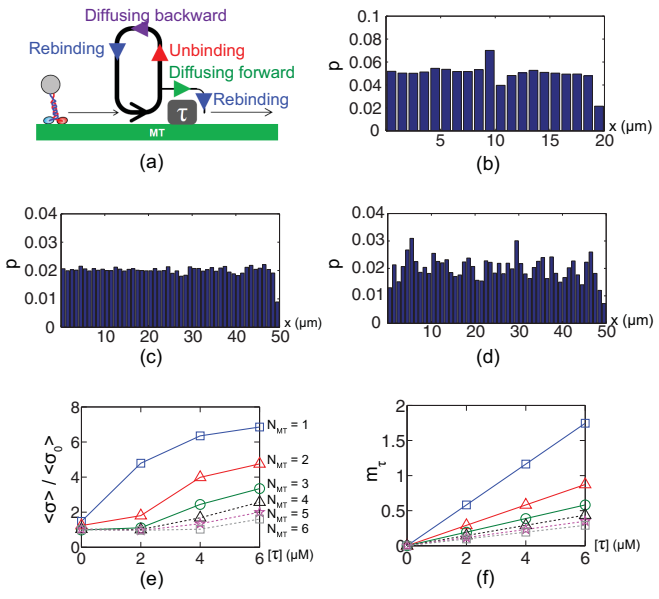

FIG. 8. Effects of tau clusters on the motion of the cargo. (a) The cycle of the motion near a tau cluster. (b) The average spatial probability distribution (ASPD) of cargoes when the tubulins located at 10 μm along the MT axis are occupied by tau clusters. Other tubulins are free of tau proteins. (c) An ASPD of an axon with $[\tau] = 0\ \mu$M and $N_{\mathrm{MT}} = 6$. (d) An ASPD of an axon with $[\tau] = 6\ \mu$M and $N_{\mathrm{MT}} = 1$. (e) The normalized mean standard deviation (std). (f) m_τ using the same symbols as in (e).

To reveal the effects of a tau cluster, tau molecules are positioned on a MT at a distance of 10 μm from its end. All other tubulins are free of tau molecules. The average spatial probability distribution (ASPD) increases in front of the cluster and decreases behind the cluster, as shown in Fig. 8(b). In the absence of tau clusters, ASPD is almost uniform along the axon, as shown in Fig. 8(c). This indicates that on average no acceleration or delay occurs at any particular location. When multiple tau clusters are present on a MT, ASPD fluctuates over the axon, as shown in Fig. 8(d).

The std of ASPD [e.g., std of probabilities shown in Figs. 8(c) and 8(d)] is calculated to quantify the spatial fluctuation of the ASPD. The ASPD and its std vary from axon to axon because the distribution of tau molecules on the MT is different over axons even when N_{MT} and $[\tau]$ are the same over axons. Thus, we simulate 20 different axons (i.e., 20 different realizations of ASPD) for each N_{MT} and $[\tau]$. Through these simulations, we also obtain 20 std values of ASPD for a given N_{MT} and $[\tau]$. The $\langle\sigma\rangle$ shown in Fig. 8(e) is the mean value of these 20 std values. Then, the $\langle\sigma\rangle$ is normalized by the mean std value $\langle\sigma_0\rangle$ corresponding to healthy axons (i.e., $N_{\mathrm{MT}} = 6$ and $[\tau] = 0\ \mu$M), as shown in Fig. 8(e). The result is surprising because the changes in std by $[\tau]$ and N_{MT} are significantly larger compared to the changes in the transport velocity depicted in Fig. 7. This strong dependency of ASPD (or std of ASPD) on $[\tau]$ and N_{MT} can be used to estimate more effectively the condition of MTs in the axon.

C. Cargo traffic in an axon

When a large number of cargoes is transported to synapses, the transport is predicted by considering the following interaction between different kinesins and between different cargoes. First, the interference between walking kinesins is taken into account using previous work [26] because that work characterizes the stepping motion of a kinesin when other kinesins are nearby. Second, effects of a bound kinesin and its cargo on an unbound kinesin are incorporated into the model by preventing the unbound kinesin from landing on the tubulins around the bound cargo. Third, the interaction among unbound cargoes can be considered by using different values of viscosity when calculating the Brownian motion of the unbound cargoes. The change in viscosity depends on the ratio between the total volume of cargoes in the axon and the volume of the axon. The volume ratio is less than 0.5% for the number of cargoes used in this study (<250). In previous studies [44], the increase in viscosity at such low volume fraction was observed to be very small (<10%). Thus, the effects of the interaction among cargoes are assumed to be negligible.

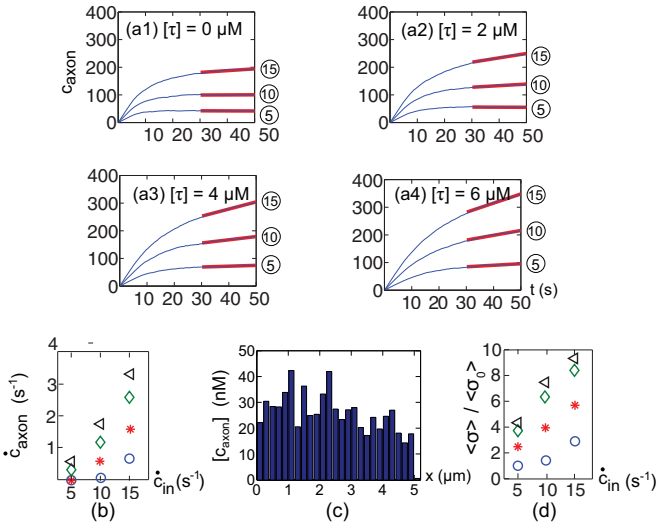

FIG. 9. Cargo traffic. (a) c_{axon} over time for $[\tau] = 0$, 2, 4, and 6 μM. Numbers shown in circles represent $\dot{c}_{\text{in}}$. N_{MT} is 1 for all these axons. (b) The rate of c_{axon} between 30 and 50 s. Circles, asterisks, diamonds, and triangles denote the rates of c_{axon} for $[\tau] = 0$, 2, 4, and 6 μM, respectively. (c) An ASCD of an axon with $\dot{c}_{\text{in}} = 5\ \text{s}^{-1}$ and $[\tau] = 6\ \mu$M. (d) The normalized mean std with the same symbols as in (b).

To study the transport, kinesins attached to cargoes are supplied near the minus end of MTs at a constant supply rate ($\dot{c}_{\text{in}}$). Then, the number of cargoes (c_{axon}) in an observation volume (i.e., 0–5-μm segment of the axon with a single MT) is captured over time. Note that the value of c_{axon} is measured for 50 s in ten different axons for each $\dot{c}_{\text{in}}$ and $[\tau]$. Then the values of c_{axon} are averaged over the axons. The changes in the traffic of cargoes over time are depicted in Fig. 9(a). In the beginning ($t < 10$ s), the number of cargoes in the observation volume increases with the supply rate ($\dot{c}_{\text{in}}$). During the time interval $10 < t < 30$ s, c_{axon} keeps increasing, but its rate of change decreases over time because some cargoes flow out of the observation volume toward the synapse with a rate of $\dot{c}_{\text{out}}$. When $t > 30$ s, the rate of change of c_{axon} is constant over time. c_{axon} does not change over time if the axonal transport system is able to transfer cargoes with the rate $\dot{c}_{\text{in}}$. Otherwise, c_{axon} increases over time with a constant rate (i.e., $\dot{c}_{\text{in}} - \dot{c}_{\text{out}}$). In the absence of tau molecules, the axon can transport cargoes toward synapses without a continuous accumulation of cargoes if $\dot{c}_{\text{in}} \leqslant 10\ \text{s}^{-1}$, as shown in Fig. 9(b). If $[\tau] = 2\,\mu$M, the cargoes accumulate in the axon if $\dot{c}_{\text{in}} \geqslant 15\ \text{s}^{-1}$. If $[\tau] = 2$ and 4 μM, the cargoes accumulate in the axon even for small $\dot{c}_{\text{in}}$ (i.e., $5\ \text{s}^{-1}$).

Similar to ASPD, averaged spatial concentration distribution (ASCD) of cargoes can be calculated using the spatial concentration distributions obtained with a uniform time sampling. The method to acquire ASCD is similar to that of ASPD. In the presence of tau molecules, ASCD fluctuates, as shown in Fig. 9(c). This result suggests that local traffic jams of cargoes are generated by tau clusters. The $\langle\sigma\rangle$ is normalized with the mean value $\langle\sigma_0\rangle$ of std for $[\tau] = 0\,\mu$M and $dot c_{\text{in}} = 5\ \text{s}^{-1}$. The normalized mean std increases significantly in the presence of tau molecules, as shown in Fig. 9(d). Also, the number of local traffic jams increases when more cargoes are injected into the axon. The local delay in transport caused by tau clusters [described in Fig. 8(a)] can be caused also by the interaction among walking kinesins and by the interference between bound cargoes and unbound cargoes. Thus, the normalized mean std for high $\dot{c}_{\text{in}}$ is large in such situations.

V. CONCLUSIONS AND DISCUSSION

Various dynamics of kinesin-mediated transport and the effects of tau protein are studied using our multiphysical model. The walking motion and unbinding motion of kinesins from MTs are considered with a previously developed model. The Brownian motion of cargoes released from the MTs is created using random numbers generated with normal distribution. This approach mitigates computational effort because this method does not require very short time steps in the simulation. Because the Brownian motion of the unbound kinesin is much faster than the random motion of their cargoes, extremely short time steps are required to capture its position. Instead, the probability for the position of unbound kinesins is used to reduce computation time. Then, the reactive zone is defined around the MTs to correlate the probability for the position of unbound kinesins and their binding probability.

The affinity of tau proteins to binding sites of MTs depends on the number of tau molecules bound on the binding sites. This behavior creates nonuniform distributions of tau molecules on the MTs. This nonuniform distribution is generated by our stochastic model to study the kinesin motion in the presence of tau protein. Then, various types of kinesin motion considered in our model are modified by the interaction between tau protein and kinesin molecule. The values of parameters are carefully determined based on several experimental observations. Therefore, our model can be used to predict the long-range transport along axons in the absence/presence of tau protein.

If cytoplasm is not crowded with kinesin molecules, the interaction between kinesin molecules is negligible. In this circumstance, the model predicts that the transport is degraded noticeable only when the density of MTs is low and the concentration of tau protein is high. When cells need to transport a large number of cargoes, the interaction between cargoes can affect the transport. An accumulation of cargoes in the axon is predicted when plenty of cargoes have to be transported. In addition, the cargoes can possibly accumulate even for relatively small number of cargoes if there is tau protein in the axon.

A key prediction obtained from our model is the local traffic jams (or delays) near tau clusters. Moreover, the results of the model suggest that this behavior can be useful for monitoring the condition of MTs. This local behavior near tau clusters is highly sensitive to the concentration of tau protein and to the density of MTs. Changes in the normalized mean std of ASPD (or ASCD) are much larger than the decrease in transport velocity. For example, when $N_{\text{MT}} = 4$ and $[\tau] = 6\ \mu$M, the velocity decreases by only 6% compared to the velocity along a healthy axon ($N_{\text{MT}} = 6$ and $[\tau] = 0\ \mu$M). However, the std of ASPD increases by 260% compared to its value in a

healthy axon. The strong dependence of ASPD on $[\tau]$ and N_{MT} can be effectively used to estimate the condition of MTs in the axon when direct observation on the condition of MT is unavailable.

Another advantage of the analysis on the local traffic jams of the transport is that it can be observed with relatively low precisions or resolutions. One can measure the binding rate, the unbinding rate, or the RL of kinesins to estimate the condition of MTs. However, a high temporal resolution and a high precision are required to observe those quantities. For example, a high temporal resolution ($<$0.01 s) is necessary to detect changes in the binding rate. Also, single particle tracking techniques with high precisions ($<$100 nm) are needed to detect changes in the RL, and that can be challenging. However, ASPD or ASCD can be obtained with relatively low temporal and spatial resolution. For example, our model predicts significant changes in ASPD by tau protein with a resolution of 0.1 s and 1 μm. These resolutions suggest that ASPD and ASCD are more effective metrics to estimate the condition of MTs than transport velocity, binding rate, and unbinding rate of kinesins.

Both transport velocity and local changes depend on the type of (obstacle) molecule interacting with kinesins on MTs and its size.

(1) In the presence of obstacle molecules which cause frequent unbinding of kinesins from MTs, the local changes near the obstacle molecules would be noticeable like the transport in the presence of tau protein. When the concentration of the molecule is not significant, the change in the transport velocity is small because unbound kinesins are able to bind to MTs in a short time.

(2) In the presence of obstacle molecules which are large but do not affect the unbinding probability of kinesins from MTs, kinesins are likely to spend a long time on MTs to bypass the large obstacle molecules. Then, both the transport velocity and local motion would change remarkably.

(3) In the presence of small obstacle molecules which do not affect unbinding probability of kinesins, both the transport velocity and local motion are not affected significantly by the molecules. By applying the interaction between obstacle molecules and kinesins, our model is able to quantitatively predict the long-range transport in the presence of different obstacle molecules.

ACKNOWLEDGMENT

This work was supported by the NSF, Civil, Mechanical, Manufacturing Innovation (CMMI) Dynamical Systems Program (Award No. 1161874).

[1] A. Brown, J. Cell Biol. **160**, 817 (2003).
[2] N. Hirokawa, Y. Noda, Y. Tanaka, and S. Niwa, Nat. Rev. Mol. Cell Biol. **10**, 682 (2009).
[3] N. Hirokawa and Y. Noda, Physiol. Rev. **88**, 1089 (2008).
[4] D. Ringe and G. A. Petsko, Cell **150**, 1093 (2012).
[5] H. Khataee and A. W.-C. Liew, Bioinformatics **30**, 353 (2014).
[6] M. J. Schnitzer, K. Visscher, and S. M. Block, Nat. Cell Biol. **2**, 718 (2000).
[7] S. M. Block, L. S. Goldstein, and B. J. Schnapp, Nature (London) **348**, 348 (1990).
[8] S. Halpain and L. Dehmelt, Genome Biol. **7**, 224 (2006).
[9] L. Dehmelt and S. Halpain, Genome Biol. **6**, 204 (2004).
[10] Z. Orbán-Németh, H. Simader, S. Badurek, A. Trančiková, and F. Propst, J. Biol. Chem. **280**, 2257 (2005).
[11] W. Stoothoff, P. B. Jones, T. L. Spires-Jones, D. Joyner, E. Chhabra, K. Bercury, Z. Fan, H. Xie, B. Bacskai, J. Edd *et al.*, J. Neurochem. **111**, 417 (2009).
[12] K. Stamer, R. Vogel, E. Thies, E. Mandelkow, and E.-M. Mandelkow, J. Cell Biol. **156**, 1051 (2002).
[13] E.-M. Mandelkow, K. Stamer, R. Vogel, E. Thies, and E. Mandelkow, Neurobiol. Aging **24**, 1079 (2003).
[14] L. A. Amos, Org. Biomol. Chem. **2**, 2153 (2004).
[15] S. Kar, J. Fan, M. J. Smith, M. Goedert, and L. A. Amos, EMBO J. **22**, 70 (2003).
[16] G. A. Petsko, Genome Biol. **13**, 176 (2012).
[17] R. Dixit, J. L. Ross, Y. E. Goldman, and E. L. Holzbaur, Science **319**, 1086 (2008).
[18] J. Xu, S. J. King, M. Lapierre-Landry, and B. Nemec, Biophys. J. **105**, L23 (2013).
[19] M. Vershinin, B. C. Carter, D. S. Razafsky, S. J. King, and S. P. Gross, Proc. Natl. Acad. Sci. USA **104**, 87 (2007).
[20] D. P. McVicker, L. R. Chrin, and C. L. Berger, J. Biol. Chem. **286**, 42873 (2011).
[21] A. Seitz, H. Kojima, K. Oiwa, E.-M. Mandelkow, Y.-H. Song, and E. Mandelkow, EMBO J. **21**, 4896 (2002).
[22] M. Ackmann, H. Wiech, and E. Mandelkow, J. Biol. Chem. **275**, 30335 (2000).
[23] W. Nam and B. I. Epureanu, J. Phys.: Condens. Matter **24**, 375103 (2012).
[24] W. Nam and B. I. Epureanu, Phys. Rev. E **86**, 051916 (2012).
[25] W. Nam and B. I. Epureanu, PLoS Comput. Biol. **11**, e1003981 (2015).
[26] W. Nam and B. I. Epureanu, PloS ONE **11**, e0147676 (2016).
[27] H. Khataee and A. W.-C. Liew, Bioinformatics, **31**, 390 (2014).
[28] J. Kerssemakers, J. Howard, H. Hess, and S. Diez, Proc. Natl. Acad. Sci. USA **103**, 15812 (2006).
[29] S. Kou, B. J. Cherayil, W. Min, B. P. English, and X. S. Xie, J. Phys. Chem. B **109**, 19068 (2005).
[30] N. Hirokawa, Y. Shiomura, and S. Okabe, J. Cell Biol. **107**, 1449 (1988).
[31] A. Peck, M. E. Sargin, N. E. LaPointe, K. Rose, B. Manjunath, S. C. Feinstein, and L. Wilson, Cytoskeleton **68**, 44 (2011).
[32] B. L. Goode, M. Chau, P. E. Denis, and S. C. Feinstein, J. Biol. Chem. **275**, 38182 (2000).
[33] E.-M. Mandelkow, J. Biernat, G. Drewes, N. Gustke, B. Trinczek, and E. Mandelkow, Neurobiol. Aging **16**, 355 (1995).
[34] U. Preuss, J. Biernat, E. Mandelkow, and E. Mandelkow, J. Cell Sci. **110**, 789 (1997).
[35] R. A. Santarella, G. Skiniotis, K. N. Goldie, P. Tittmann, H. Gross, E.-M. Mandelkow, E. Mandelkow, and A. Hoenger, J. Mol. Biol. **339**, 539 (2004).

[36] S. Konzack, E. Thies, A. Marx, E.-M. Mandelkow, and E. Mandelkow, J. Neurosci. **27**, 9916 (2007).
[37] P. Friedhoff, M. Von Bergen, E.-M. Mandelkow, P. Davies, and E. Mandelkow, Proc. Natl. Acad. Sci. USA **95**, 15712 (1998).
[38] S. P. Gilbert, M. R. Webb, M. Brune, and K. A. Johnson, Nature (London) **373**, 671 (1995).
[39] G. S. Bloom, M. C. Wagner, K. K. Pfister, and S. T. Brady, Biochemistry **27**, 3409 (1988).
[40] S. Popov and M. Poo, J. Neurosci. **12**, 77 (1992).
[41] D. Barazany, P. J. Basser, and Y. Assaf, Brain **132**, 1210 (2009).
[42] A. D. Cash, G. Aliev, S. L. Siedlak, A. Nunomura, H. Fujioka, X. Zhu, A. K. Raina, H. V. Vinters, M. Tabaton, A. B. Johnson *et al.*, Am. J. Pathol. **162**, 1623 (2003).
[43] K. Visscher, M. J. Schnitzer, and S. M. Block, Nature (London) **400**, 184 (1999).
[44] C. Nguyen, F. Desgranges, G. Roy, N. Galanis, T. Mare, S. Boucher, and H. Angue Mintsa, Int J. Heat Fluid Flow **28**, 1492 (2007).